AIP | The Journal of Chemical Physics

# Slow photoelectron velocity-map imaging spectroscopy of the Fe3O– and Co3O– anions

Jongjin B. Kim, Marissa L. Weichman, and Daniel M. Neumark

Citation: The Journal of Chemical Physics **141**, 174307 (2014); doi: 10.1063/1.4900646
View online: http://dx.doi.org/10.1063/1.4900646
View Table of Contents: http://scitation.aip.org/content/aip/journal/jcp/141/17?ver=pdfcov
Published by the AIP Publishing

# Slow photoelectron velocity-map imaging spectroscopy of the $Fe_3O^-$ and $Co_3O^-$ anions

Jongjin B. Kim, Marissa L. Weichman, and Daniel M. Neumark[a)]
*Department of Chemistry, University of California, Berkeley, California 94720, USA and*
*Chemical Sciences Division, Lawrence Berkeley National Laboratory, Berkeley, California 94720, USA*

(Received 7 September 2014; accepted 17 October 2014; published online 4 November 2014)

We report high-resolution photoelectron spectra of the transition metal suboxide clusters $Fe_3O^-$ and $Co_3O^-$. The combination of slow electron velocity-map imaging and cryogenic cooling yields vibrationally well-resolved spectra, from which we obtain precise values of 1.4408(3) and 1.3951(4) eV for the electron affinities of $Fe_3O$ and $Co_3O$. Several vibrational frequencies of the neutral ground state $Fe_3O$ and $Co_3O$ clusters are assigned for the first time, and a low-lying excited state of $Fe_3O$ is observed. The experimental results are compared with density functional electronic structure calculations and Franck-Condon spectral simulations, enabling identification of the structural isomer and electronic states. As has been found in photoelectron spectra of other trimetal oxo species, $Fe_3O^{0/-}$ and $Co_3O^{0/-}$ are assigned to a $\mu_2$-oxo isomer with planar $C_{2v}$ symmetry. We identify the ground states of $Fe_3O^-$ and $Co_3O^-$ as $^{12}A_1$ and $^9B_2$ states, respectively. From these states we observe photodetachment to the $^{11}B_2$ ground and $^{13}A_1$ excited states of $Fe_3O$, as well as to the $^8A_1$ ground state of $Co_3O$. © *2014 AIP Publishing LLC*. [http://dx.doi.org/10.1063/1.4900646]

## I. INTRODUCTION

The properties of iron and cobalt oxides have been of interest for many years. Iron oxide-based materials are used for dehydrogenation catalysis, stimulating many bulk structural and reactivity studies in an effort to understand the underlying chemistry.[1] While the primary industrial role of cobalt oxides are as pigments, these species have long been studied for potential uses in oxidation catalysis.[2,3] Recent developments in artificial photosynthesis have also found that self-assembled cobalt-oxo-based materials can be a self-healing, oxygen-evolving catalyst.[4] Understanding the fundamental properties of iron and cobalt oxides that govern their reactivity is a daunting task, made even more difficult by the fact that the reactivity of these inhomogeneous bulk materials will depend on the local geometry. These considerations have motivated gas-phase mass spectrometry studies on size-selected iron and cobalt oxide clusters, which have found dramatic effects in their chemistry as a function of size, charge, and stoichiometry.[5–19] Interpreting these results requires spectroscopic experiments that can elucidate the energetics and structures of the clusters,[20–22] a challenging task for clusters comprising multiple metal atoms that requires novel instrumentation. Here, we report vibrationally resolved photoelectron spectra of the trimetal clusters $Fe_3O^-$ and $Co_3O^-$ via slow-electron velocity-map imaging (SEVI) of cryogenically cooled anions and, with the aid of density-functional calculations, assign the vibrational structure and ground electronic states of the anionic and neutral clusters.

Spectroscopy of iron and cobalt oxides has been extensively carried out for the diatomic metal oxides with a variety of techniques.[23,24] However, similar studies of the polymetal clusters have been historically limited; beyond the smallest species, a mix of cluster sizes is often produced, and thus mass-selection must almost always be coupled to a sensitive spectroscopic technique. The most successful methods for probing gas-phase metal oxide clusters have been based on IR photodissociation (IRPD) or anion photoelectron (PE) spectroscopy. In IRPD spectroscopy, anions or cations are mass-selected and fragmented with IR light resonant with vibrational modes; the photofragment yield is taken as a measure of the vibrational absorption spectrum.[20,25] In anion PE spectroscopy, anions are mass-selected then photodetached; the measured kinetic energy distribution of the electrons gives information of the neutral vibronic structure.[26] Conventional anion PE spectroscopy with an electrostatic or time-of-flight energy analyzer has been limited to a typical resolution of ~100 $cm^{-1}$, often only providing partially resolved vibrational spectra of metal oxide clusters,[27–29] but the development of slow electron velocity-map imaging (SEVI) has improved this to just a few wavenumbers,[30–32] allowing for detailed vibrational information on previously poorly characterized metal oxides.[33,34] The related technique of threshold photoionization spectroscopy has been useful in studying neutral and cation metal oxide clusters, either through mass-analyzed threshold ionization (MATI),[35,36] or at sub-meV resolution by using zero-kinetic energy (ZEKE) spectroscopy.[37]

For the $Fe_3O^{0/-}$ and $Co_3O^{0/-}$ clusters, the only spectroscopic studies reported have used anion PE spectroscopy,[38–40] although magnetic deflection experiments of iron and iron-oxo clusters have also suggested that $Fe_3O$ is a ferromagnetic species.[41] No vibrational structure was observed in the

a)Author to whom correspondence should be addressed. Electronic mail: dneumark@berkeley.edu

 

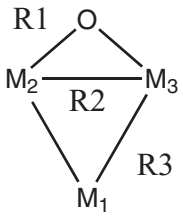


FIG. 1. Schematic structure of the $C_{2v}$-symmetric $M_3O^{0/-}$ species (M = Fe, Co), with labels shown for the bond lengths R1, R2, R3 listed in Table S2 in the supplementary material and metal atoms listed in Table S3 in the supplementary material.[62]

PE spectra; the photodetachment transitions were assigned by comparison of the observed detachment energies with calculated values. Vibrationally-resolved anion PE and neutral ZEKE studies have been reported on a few similar trimetal oxide species; Leopold and co-workers used anion PE spectroscopy on the Group 5 oxides $M_3O^-$ (M = V, Nb, Ta),[42] while Yang and co-workers used ZEKE to probe the vibrational structure of $Nb_3O^{0/+}$ and $Zr_3O^{0/+}$.[37,43] In all these cases, the observed Franck-Condon structure was a key element in assigning relevant states in the detachment and ionization transitions. Regardless of the metal, they also all supported a structural isomer with a triangular metal moiety and a $\mu_2$-oxo, as shown in Fig. 1.

Theoretical studies on larger $Fe_3O^{0/-}$ and $Co_3O^{0/-}$ clusters have been limited to density functional calculations. The anion and neutral $Fe_3O$ clusters have been studied by the BPW91 and PW91 generalized gradient approximations (GGAs).[38,44,45] The most stable isomer was calculated to have a $Fe_3$ triangular moiety with a bridging $\mu_2$-oxo on the edge (Fig. 1). The lowest-energy state of $Fe_3O$ was predicted to have a spin multiplicity $2S + 1$ of 11, and that of $Fe_3O^-$ to have a multiplicity of 12. The $Co_3O$ clusters have been studied with the B3LYP hybrid functional as well as the BPW91 and PBE GGA functionals.[39,46,47] While the $\mu_2$-oxo isomer was found to be the most stable form of $Co_3O^{0/-}$ with BPW91 and of neutral $Co_3O$ with PBE, another isomer with an inserted oxygen was found to be most stable form of neutral $Co_3O$ with B3LYP.

In this work, we elucidate the electronic and vibrational structures of $Fe_3O^{0/-}$ and $Co_3O^{0/-}$ through a combination of high-resolution anion PE spectroscopy and density functional theory (DFT) calculations. Compared to previous anion PE reports, we used a high-resolution slow electron velocity-map imaging (SEVI) spectrometer combined with a cryogenic ion trap, allowing for the acquisition of vibrationally well-resolved spectra. These are compared to energetics and Franck-Condon simulations, allowing us to assign the $Fe_3O^-$ and $Co_3O^-$ detachment transitions. Electron affinities are improved from prior studies, and various vibrational frequencies are assigned for the first time. Both trimetal oxo species in both charge states are found to have a triangular metal motif with a bridging oxo (Fig. 1). The ground states of $Fe_3O^-$ and $Co_3O^-$ are identified as $^{12}A_1$ and $^9B_2$ states, respectively, while $Fe_3O$ and $Co_3O$ have $^{11}B_2$ and $^8A_1$ ground states. We also tentatively identify a low-lying $^{13}A_1$ excited state of $Fe_3O$.

## II. EXPERIMENTAL METHODS

The photoelectron spectra were acquired with our high-resolution SEVI instrument, which has been described in detail previously.[30,31,48] Metal oxide cluster anions were produced by a laser ablation source, cooled by a cryogenic ion trap, mass selected, and photodetached. The resulting photoelectrons were collected and imaged by an electrostatic lens, with relatively low potentials chosen such that low-eKE, high-resolution spectra were captured.

$Fe_3O^-$ and $Co_3O^-$ ions were produced by laser ablation of steel or cobalt, respectively. At a 20 Hz repetition rate, a 2–10 mJ laser pulse of 532 nm light was focused onto the solid target, and a burst of helium gas with trace oxygen from a pulsed valve was used to quench the plasma and create metal oxide clusters. The anions were mass-selected in a quadrupole mass filter that transmitted the $^{56}Fe_3{}^{16}O^-$ or $^{59}Co_3{}^{16}O^-$ clusters and were then transferred to an ion trap. There, the ions were cooled by a 1:4 mix of $H_2$/He buffer gas at 5 K for 40 ms.

The ions were extracted from the trap and accelerated in a time-of-flight mass spectrometer. When the ion packets reached the interaction volume of the velocity-map imaging (VMI) electron spectrometer,[49] they were photodetached with the output from a tunable pulsed dye laser. The VMI lens projected the resulting photoelectrons onto a planar position-sensitive detector; a single image results from the accumulation of photoelectrons from several thousand experimental cycles. As a unique axis is defined by the laser polarization axis, the projected image can be used to reconstruct the original electron velocity distribution, allowing us to obtain radial and angular information.[50]

The radial photoelectron distribution is proportional to the speed; this distribution gives the electron kinetic energy (eKE) distribution at a given photon energy. As detailed previously,[51] we obtain the highest resolution at lowest eKE, so the high-resolution, low-eKE portions of individual scans were spliced together and scaled to match the intensities from a lower resolution overview spectrum covering a broad range of eKE. For a more useful quantity, we report the energies as electron binding energies (eBE), defined as eBE = $h\nu$ − eKE, which give the energy difference between the anion and neutral states.

We also measure photoelectron angular distributions (PADs), which for a one-photon detachment with linearly polarized light can be described by the formula,[52]

$$\frac{d\sigma}{d\Omega} = \frac{\sigma_{tot}}{4\pi}\left(1 + \beta\left(\frac{3}{2}\cos^2\theta - \frac{1}{2}\right)\right). \quad (1)$$

The anisotropy of the PAD is defined by the parameter $\beta$, which varies from −1 to 2, corresponding to the limits of a PAD aligned perpendicular to and parallel to the photon polarization. For a given transition, the value of $\beta$ depends on the photodetachment energy. However, its qualitative value can give insight to the nature and symmetry of the photodetachment transition.[53,54] In this work, peaks with $0.1 < \beta < 2$ are labeled with a "+" PAD while those with $-1 < \beta < 0.1$ are labeled with a "−" PAD.

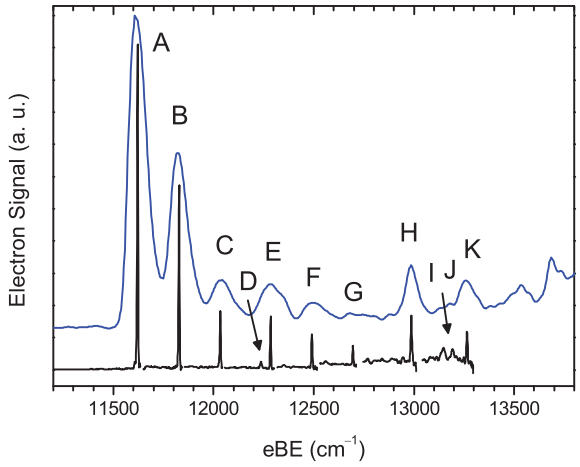


FIG. 2. SEVI spectra of $Fe_3O^-$. The upper blue trace is an overview spectrum taken at a photon energy of 14 925 $cm^{-1}$ and shifted vertically for clarity, while the black segments are high-resolution portions of scans taken at lower photon energies.

## III. RESULTS

SEVI spectra of $Fe_3O^-$ and $Co_3O^-$ are shown in Figs. 2 and 3, respectively. Lower-resolution overview spectra are shown in top (blue), composed of an average of several scans taken near photon energies of 14 925 $cm^{-1}$ and 13 339 $cm^{-1}$. The high-resolution portions of SEVI spectra taken at various photon energies are spliced together below (black), highlighting the better-resolved vibrational structure at low eKE.

The overview spectra for $Fe_3O^-$ and $Co_3O^-$ are similar; both have a strong vibrational origin at peak A and a short progression comprising peaks A, B, and C, with a peak spacing of ~210 $cm^{-1}$ and ~190 $cm^{-1}$, respectively. There appears to be a minor recurrence of this progression starting at peak E, ~660 $cm^{-1}$ higher in energy. Almost all features have a characteristic "−" PAD, but peaks H and K in the $Fe_3O^-$ spectrum have a "+" PAD, suggesting the onset of a new electronic band.

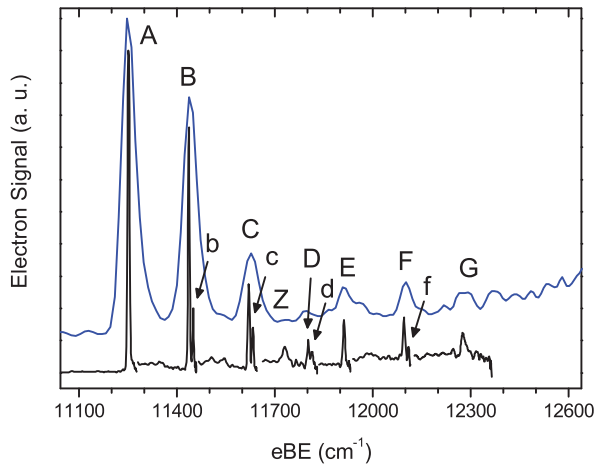


FIG. 3. SEVI spectra of $Co_3O^-$. The upper blue trace is an overview spectrum taken at a photon energy of 13 341 $cm^{-1}$ and shifted vertically for clarity, while the black segments are high-resolution portions of scans taken at lower photon energies.

TABLE I. Peak positions ($cm^{-1}$), shifts from the origin ($cm^{-1}$), characteristic PADs, and assignments for the $Fe_3O^-$ SEVI spectra.

| Peak | eBE | Shift | PAD | Assignment |
|---|---|---|---|---|
| A | 11 620 | 0 | – | $0_0^0$ |
| B | 11 828 | 207 | – | $3_0^1$ |
| C | 12 034 | 413 | – | $3_0^2$ |
| D | 12 237 | 616 | – | $3_0^3$ |
| E | 12 285 | 664 | – | $1_0^1$ |
| F | 12 491 | 870 | – | $1_0^1 3_0^1$ |
| G | 12 695 | 1075 | – | $1_0^1 3_0^2$ |
| H | 12 987 | 1367 | + | $\tilde{a}\, 0_0^0$ |
| I | 13 146 | 1525 | | |
| J | 13 193 | 1572 | | |
| K | 13 265 | 1644 | + | $\tilde{a}\, 2_0^1$ |

Higher-resolution spectra resolve the observed features in the $Fe_3O^-$ spectrum more clearly and show new features in the $Co_3O^-$ spectrum. The $Fe_3O^-$ spectra are still dominated by two main progressions comprising peaks A-D and E-G with a peak spacing of ~210 $cm^{-1}$ and separated by ~660 $cm^{-1}$. Peaks I and J are resolved between peaks H and K, but poor signal-to-noise prevents assignment of their PAD. The $Fe_3O^-$ spectra are congested above peak K, and high-resolution spectra at higher energies are not shown. In the $Co_3O^-$ spectra, the main features are still the A-D and E-G progressions. The peaks above the onsets A and E, however, are now resolved as doublets, with the weak peaks b, c, d, and f observed 13 $cm^{-1}$ above the corresponding stronger peaks B, C, D, and F. A weak but reproducible (and thus far unassigned) feature is also observed between peaks C and D and is labeled peak Z.

Peak positions, PADs, and assignments are summarized in Tables I and II for the $Fe_3O^-$ and $Co_3O^-$ SEVI spectra. Typical peak widths are 6 $cm^{-1}$ FWHM and peak position errors are no more than 2–3 $cm^{-1}$.

TABLE II. Peak positions ($cm^{-1}$), shifts from the origin ($cm^{-1}$), characteristic PADs, and assignments for the $Co_3O^-$ SEVI spectra.

| Peak | eBE | Shift | PAD | Assignment |
|---|---|---|---|---|
| A | 11 252 | 0 | – | $0_0^0$ |
| B | 11 437 | 185 | – | $3_0^1$ |
| b | 11 450 | 198 | – | $4_0^2$ |
| C | 11 621 | 369 | – | $3_0^2$ |
| c | 11 633 | 381 | – | $3_0^1 4_0^2$ |
| Z | 11 731 | 479 | – | |
| D | 11 803 | 551 | – | $3_0^3$ |
| d | 11 814 | 562 | – | $3_0^2 4_0^2$ |
| E | 11 912 | 660 | – | $1_0^1$ |
| F | 12 096 | 844 | – | $1_0^1 3_0^1$ |
| f | 12 110 | 857 | – | $1_0^1 4_0^2$ |
| G | 12 279 | 1026 | – | $1_0^1 3_0^2$ |

## IV. THEORETICAL RESULTS

### A. Electronic structure theory

Previous calculations on $Fe_3O^{0/-}$ and $Co_3O^{0/-}$ have used the BPW91 functional with a 6-311+G* basis set, with reasonable agreement between the calculated and experimental EAs and assignment of a $\mu_2$-oxo isomer.[38,39] Calculations with the PW91 functional found similar results for $Fe_3O^{0/-}$.[44,45] Another study found a different ground state isomer for $Co_3O$,[46] but used smaller double-zeta basis sets and the B3LYP hybrid functional, while a calculation with the PBE functional found the same $\mu_2$-oxo isomer for $Co_3O$.[47] While BPW91 calculations reported use the same functional and basis set, they may differ in various parameters like the quadrature integration grid; a sufficiently fine grid is necessary for converged results at a given functional and basis set, especially for transition-metal systems and with some newer functionals.[55,56]

For consistency, we performed an independent set of calculations of all species, also at the BPW91/6-311+G* level, with tight geometry optimization and an ultrafine integration grid as defined by Gaussian 09.[57] The TPSS meta-GGA functional[58] can have improved performance depending on the system and parameters studied,[59] and a recent study of the difficult $FeO_2^+$ system found that of the functionals tested, only TPSS qualitatively agreed with high-level multireference *ab initio* theory.[60] Accordingly, geometry optimizations and frequency calculations were also performed at TPSS/6-311+G*. Calculations were performed with and without symmetry, and wavefunction stability was enforced by the diagnostic in Gaussian. For interpreting the nature of the electronic states, a Natural Population Analysis was performed on selected states with the TPSS functional.[61]

Fig. 4 shows the calculated energies of the three lowest-lying states of the $\mu_2$-oxo isomer for neutral and anionic $Fe_3O$ and $Co_3O$. Numerical values and calculated $\langle S^2 \rangle$ values are given in Table S1 of the supplementary material.[62] All states shown here have only minor deviations between $\langle S^2 \rangle$ and the ideal $S(S+1)$ value, suggesting there is only minor spin contamination and that DFT may provide a reasonable treatment for these systems. Moreover, the relative energies of all the states are similar between BPW91 and TPSS; these self-consistent results between different functionals suggest that the energies are reliable. Calculated geometries and harmonic vibrational frequencies from both functionals are reported in Table S2 in the supplementary material, while the results of the Natural Population Analysis are shown in Table S3 in the supplementary material.[62]

All states converge to a planar $C_{2v}$ geometry except the sextet $^6A''$ $Co_3O$ state, for which the oxygen atom is found to be out of the $Co_3$ plane by 46.5° by both BPW91 and TPSS. While the $Fe_3O$ $^9A_1$ state and $Co_3O$ $^8A_1$ state have imaginary frequencies using the TPSS and BPW91 functionals, respectively, the relaxation energy by breaking symmetry is only 14 $cm^{-1}$ and 1 $cm^{-1}$, well below the zero-point vibrational energy, and we consider them to be $C_{2v}$. The normal mode coordinates for all species are similar; those of an exemplar ($Fe_3O$, $^{11}B_2$ state) are displayed in Fig. 5.

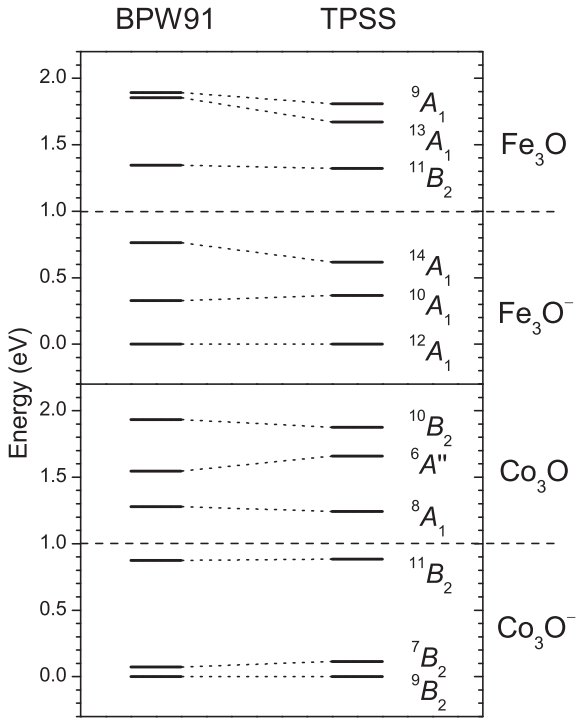


FIG. 4. Energy level diagram of the low-lying $Fe_3O^{0/-}$ and $Co_3O^{0/-}$ states calculated using the BPW91 and TPSS functionals. All energies are relative to the lowest-energy anion state.

We considered the possibility of alternative structural isomers and optimized for the various $M_3O$ isomers considered in previous studies.[39,46,47] However, regardless of metal and charge, all alternate isomers were found significantly higher in energy than the ground state, with the lowest-lying alternate isomer 0.33 eV higher in energy than the corresponding ground state, a neutral octet $Co_3O$ isomer with a $\mu_3$-oxo pyramidal motif. Our calculations support the $\mu_2$-oxo isomer for these species.

### B. Franck-Condon simulations

To aid in the assignment of our spectra, Franck-Condon (FC) simulations of the possible photodetachment transitions were calculated with the ezSpectrum program.[63] With this program, all modes are mixed with Duschinsky rotation and overlap integrals are calculated in the harmonic oscillator

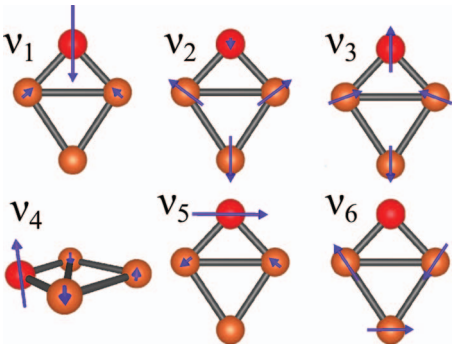


FIG. 5. Vibrational normal modes of the $M_3O$ species.

approximation. Only photodetachment transitions with $\Delta S = 1/2$ are allowed and thus have their spectra simulated in this work. Calculated spectra are compared to experimental overview spectra in Figs. 6 and 7 for $Fe_3O^-$ and $Co_3O^-$, respectively. The stick spectra are displayed as well as spectra convolved with the instrumental resolution matching that of the overview spectrum, $\Delta E/E = 3\%$.

However, the $\nu_4$ $b_1$ mode of the $Co_3O$ $^8A_1$ state is treated separately as an anharmonic oscillator and is left out of the ezSpectrum FC simulations. The frequency of this mode varies significantly with charge, state, and density functional. In particular, in the $^8A_1$ state this mode has a small real frequency of 28 $cm^{-1}$ with TPSS and a small imaginary harmonic frequency of $32i$ $cm^{-1}$ using BPW91. This behavior is suggestive of a flat anharmonic potential along that mode. As a non-totally symmetric mode, $\Delta v_4 =$ odd transitions are forbidden, but if the anharmonicity is sufficiently pronounced or the frequency changes a large degree between the initial and final states, $\Delta v_4 = 2$ excitation may have significant FC intensity. This treatment is discussed more thoroughly in Sec. V B.

## V. DISCUSSION

### A. Assignment of $Fe_3O^-$ spectra

Peak A is assigned as the vibronic origin of the main photodetachment band; no features appear lower in energy, and as the ions were cooled in a cryogenic trap, the lowest-energy feature should correspond to the origin. All electronic structure calculations in this work and most previous theory support a $\mu_2$-oxo triangular metal isomer for the $M_3O^{0/-}$ species here.[38,44,45] Moreover, experimental studies of analogous trimetal oxo compounds using vibrationally resolved ZEKE and conventional anion PE spectroscopy studies have also been assigned to this structural isomer.[37,42,43] Those spectra were similar in appearance to ours, with a strong vibrational origin and weak FC activity in just a few modes. These considerations suggest that $Fe_3O^{0/-}$ has the structural motif shown in Fig. 1, but comparison must be made between experimental and calculated spectra for an unambiguous determination.

We compare our results to calculated vibrational frequencies and Franck-Condon profiles. The FC-active modes of the $\mu_2$-oxo structure are the totally symmetric $\nu_1$, $\nu_2$, and $\nu_3$ modes (Fig. 5). Regardless of functional and spin state chosen, the calculated harmonic frequencies $\omega_1$, $\omega_2$, and $\omega_3$ for these modes lie within a narrow range: $\omega_1 \sim$ 630–680 $cm^{-1}$, $\omega_2 \sim$ 320–340 $cm^{-1}$, and $\omega_3 \sim$ 200–230 $cm^{-1}$ (Table S2 in the supplementary material).[62] The experimental spectra show two progressions A-D and E-G, which are characteristic of Franck-Condon activity in two vibrational modes with frequencies ~210 $cm^{-1}$ and 660 $cm^{-1}$. By comparison with the calculated frequencies, there is a clear match for the $\nu_1$ and $\nu_3$ modes, supporting the validity of the calculated structure in Fig. 1, and allowing us to assign peaks A-D to the $3_0^n$ (n = 0–3) progression, and peaks E-G to the $1_0^1 3_0^n$ (n = 0–2) progression.

Peaks H and K exhibit a different PAD than peaks A-G, suggesting a photodetachment transition with different electronic character. Assuming that ion trapping and cooling ensure that all the anions are in their ground electronic state, Peak H is assigned as the origin of a transition to an excited neutral state, lying 1300 $cm^{-1}$ above the state responsible for the main band. Peak K is offset from peak H by 278 $cm^{-1}$; by comparison with the calculated vibrational frequencies, this suggests a tentative $2_0^1$ assignment in the excited state.

While assigning the vibrational structure is straightforward, a comparison of Franck-Condon activity is required for assignment of the electronic states. The calculations suggest that the ground states of anionic and neutral $Fe_3O$ should be the $^{12}A_1$ and $^{11}B_2$ states, respectively. However, excited states are calculated to lie only a few tenths of an eV higher in energy. Nevertheless, we can use the Franck-Condon activity as a means to verify the reliability of calculations; if both the calculated energies and FC simulation are consistent with experiment, the electronic state assignment is likely to be correct.

FC simulations of $Fe_3O^-$ photodetachment are shown in Fig. 6, with all possible one-electron detachment transitions between the states in Fig. 4 considered. To a first approximation, all the simulations are reasonable matches; the vibrational origin is the first or second most intense peak, consistent with the expectations provided from previous photoelectron studies of similar systems.[37,42] However, the simulated $^{11}B_2 \leftarrow {}^{12}A_1$ transition is clearly a better match to the experiment than the other transitions. The intensities of the $3_0^n$ and $1_0^1 3_0^n$ progressions are well-reproduced, and there is negligible excitation in the $\nu_2$ mode, consistent with the experimental spectra. Those two states are also calculated to be the lowest energy states of the neutral and anion $Fe_3O$, respectively, and the calculated EA is around 1.33 eV (Table S1 in the supplementary material),[62] in reasonable agreement with the eBE of peak A at 1.4408 eV. The good match of calculated energies, FC activity, and experimental spectra leads us to assign the anion and neutral ground states as the $\tilde{X}$ $^{12}A_1$ and $\tilde{X}$ $^{11}B_2$ states, respectively, and the main photodetachment band to the transition between these two states.

The assignment of the excited state beginning at peak H is more tentative. As the anion is now established as a $^{12}A_1$ state, we need only consider undectet and tridectet states of neutral $Fe_3O$. As we have not performed excited-state calculations, we cannot rule out the presence of an excited undectet state. However, the lowest-lying tridectet state, a $^{13}A_1$ state, is calculated to lie only 0.51 or 0.35 eV above the ground state, depending on the functional used. Peak H is offset from the ground state origin by 0.1694 eV, a smaller value than the calculated term energy, but within reasonable error of DFT.

Unfortunately, the experimental FC activity is not as well-resolved for this band, as the spectra are congested above peak K. Nevertheless, it is sufficient to determine that peak H and K have roughly comparable intensities, and peak K is tentatively assigned as a $2_0^1$ transition. It is possible that one of peaks I and J correspond to a $3_0^1$ transition, but peak positions compared to calculated frequencies are ambiguous; regardless, $\nu_3$ activity is at most minor relative to $\nu_2$ activity. The $^{13}A_1 \leftarrow \tilde{X}$ $^{12}A_1$ FC simulation is a reasonable match to these

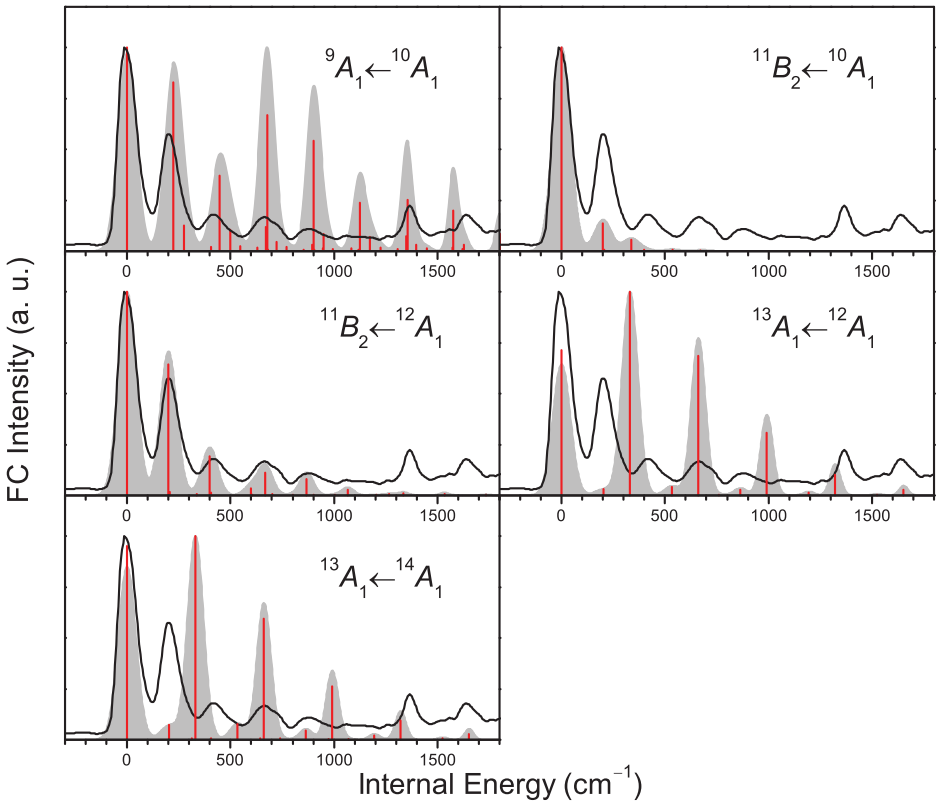


FIG. 6. FC simulations of the main photodetachment band for all possible $Fe_3O^-$ detachment transitions with $\Delta S = 1/2$ and with the states considered in this work. The black trace is the same experimental overview spectrum in Fig. 2 for comparison with the simulated stick spectra (red) and simulation at experimental resolution (grey), shifted so the vibrational origin is at zero energy. All spectra are normalized to the same maximum intensity. Experimental features above 1300 cm$^{-1}$ are assigned to an excited state and should not be compared to simulations.

observations, with weak $\nu_3$ activity, stronger $\nu_2$ activity, and a roughly comparable intensity between the $0_0^0$ and $2_0^1$ transitions. We tentatively assign peaks H and K to the $Fe_3O$ $\tilde{a}\ ^{13}A_1$ state.

Photoelectron anisotropies and threshold intensities are consistent with the assignments of both bands. Qualitative predictions of the PAD can be made using the Wigner Threshold Law: at low eKE, the photodetachment cross-section for negative ions goes as $\sigma \propto \text{eKE}^{l+1/2}$, where $l$ is the orbital angular momentum of the detached electron.[64] Hence, only the lowest-order partial waves contribute significantly to photodetachment near threshold. Considering only the $l = 0$ and $l = 1$ waves, we can use a model developed by Sanov and co-workers to predict the sign of the PAD for polyatomic species.[53,65] For $C_{2v}$ systems like the $M_3O$ species considered in this work, only detachment from an $a_1$ orbital would exhibit a "+" PAD, and while detachment from an $a_2$, $b_1$, or $b_2$ orbital would have a "−" PAD. Moreover, as the $A_2$ irreducible representation does not contain any $x$, $y$, or $z$ components, detachment from an $a_2$ orbital would proceed by $l = 1$ in the lowest order and thus would drop off in intensity at very low eKE.[51,66] All peaks maintained reasonable intensity close to threshold, consistent with s-wave ($l = 0$) detachment and ruling out detachment from an $a_2$ orbital. The $\tilde{X}\ ^{11}B_2 \leftarrow \tilde{X}\ ^{12}A_1$ transition has a "−" PAD consistent with detachment from a $b_2$ orbital, while the $\tilde{a}\ ^{13}A_1 \leftarrow \tilde{X}\ ^{12}A_1$ transition has a "+" PAD consistent with detachment from an $a_1$ orbital.

The assigned states, state energies, and vibrational frequencies are summarized in Table III. We report only the vibrational fundamentals for $Fe_3O$.

### B. Assignment of $Co_3O^-$ spectra

As in the $Fe_3O^-$ spectra, peak A is the lowest-eBE and most intense feature, so it is assigned to the vibrational origin of the main photodetachment band. The overall vibrational structure is similar, also suggesting the same $\mu_2$-oxo structural isomer. However, the finer vibrational structure is characteristic of FC activity in three modes, not just two. The main progressions A-D and E-G once again suggest vibrational

TABLE III. Experimental vibrational frequencies and electronic state energies for $Fe_3O$ and $Co_3O$.

| | $Fe_3O$ | $Co_3O$ |
|---|---|---|
| Anion | $^{12}A_1$ | $^9B_2$ |
| $\tilde{X}$ | $^{11}B_2$ | $^8A_1$ |
| EA (eV) | 1.4408(3) | 1.3951(4) |
| $\nu_1$ (cm$^{-1}$) | 664(2) | 660(3) |
| $\nu_3$ (cm$^{-1}$) | 207(2) | 185(2) |
| $2\nu_4$ (cm$^{-1}$) | | 198(2) |
| $\tilde{a}$ | $^{13}A_1$ | |
| $T_0$ (eV) | 0.1694(4) | |
| $\nu_2$ (cm$^{-1}$) | 278(3) | |

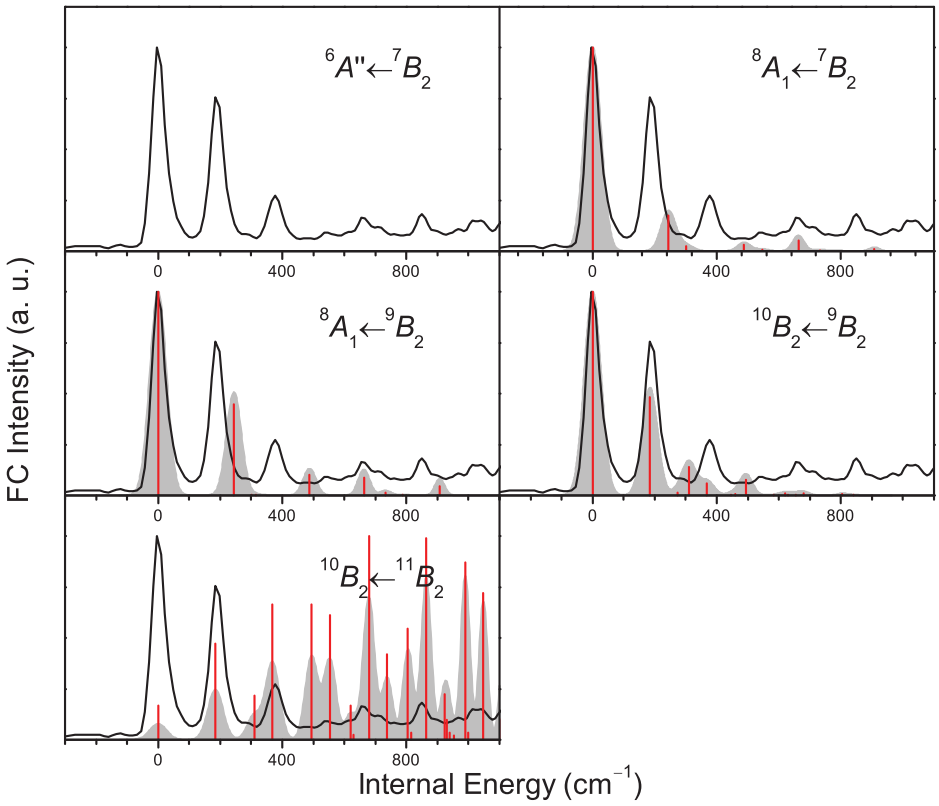


FIG. 7. FC simulations of the main photodetachment band for all possible $Co_3O^-$ detachment transitions with $\Delta S = 1/2$ and with the states considered in this work. The black trace is the same experimental overview spectrum in Fig. 3 for comparison with the simulated stick spectra (red) and simulation at experimental resolution (grey), shifted so the vibrational origin is at zero energy. All spectra are normalized to the same maximum intensity, except for the $^6A''$ $\leftarrow {}^7B_2$ transition, which has negligible intensity in the displayed energy range owing to a large geometry change.

activity in two modes with frequencies ~190 $cm^{-1}$ and ~660 $cm^{-1}$. The spread of calculated frequencies is larger than in $Fe_3O$, with the various harmonic frequencies of neutral $Co_3O$ spanning 617–665 $cm^{-1}$, 286–322 $cm^{-1}$, and 184–244 $cm^{-1}$ for $\omega_1$, $\omega_2$, and $\omega_3$, respectively. Nevertheless, we can once again match peak spacings to progressions in the $\nu_1$ and $\nu_3$ modes. We assign peaks A-D to the $3_0^n$ (n = 0–3) progression, and peaks E-G to the $1_0^1 3_0^n$ (n = 0–2) progression.

Before considering the additional structure, we compare FC simulations with experiment to narrow down the states of interest. All FC simulations of the possible $Co_3O^-$ detachment transitions are shown in Fig. 7. Surprisingly, unlike the case with $Fe_3O^-$, two of the five transitions have weak vibrational origins. Most dramatically, the $^6A'' \leftarrow {}^7B_2$ transition has negligible calculated FC intensity in the area shown, due to the large change in geometry from a planar to nonplanar structure, and the $^{10}B_2 \leftarrow {}^{11}B_1$ simulation is also very extended. The other three transitions, however, have the expected strong origin and moderate FC activity. In more detail, the $^8A_1 \leftarrow {}^7B_2$ simulation exhibits notably less FC activity than the experimental spectrum, but the $^8A_1 \leftarrow {}^9B_2$ and $^{10}B_2 \leftarrow {}^9B_2$ transitions qualitatively match the experimental overview spectrum. Neither is as good a match as the $Fe_3O^-$ $^{11}B_2 \leftarrow {}^{12}A_1$ simulation, however. The $^8A_1 \leftarrow {}^9B_2$ simulation is dominated by a progression in the $\nu_3$ mode but the calculated frequency of 244 $cm^{-1}$ is larger than our experimental value of 185 $cm^{-1}$. The $^{10}B_2 \leftarrow {}^9B_2$ simulation has insignificant $\nu_1$ activity, but both $\nu_2$ and $\nu_3$ modes are active, in disagreement with the experiment showing no activity in the $\nu_2$ mode.

Differentiating between the likeliest $^8A_1 \leftarrow {}^9B_2$ or $^{10}B_2 \leftarrow {}^9B_2$ transitions requires consideration of angular information. The PADs of all listed peaks are qualitatively similar, consistent with a common electronic transition for these peaks. All features have a characteristic "−" PAD, consistent with that expected for detachment from a $b_2$ orbital and thus supports assignment to the $^8A_1 \leftarrow {}^9B_2$ transition. The $^{10}B_2 \leftarrow {}^9B_2$ transition, however, occurs by detachment from an $a_1$ orbital and would be expected to have a "+" PAD.

Assignment of the $^8A_1 \leftarrow {}^9B_2$ transition by the PAD also allows for an explanation of the doublet structure in the spectra from even quanta excitation of the $\nu_4$ mode. The weak peaks b, c, d, and f neighboring the main progressions suggest weak excitation in another mode with a frequency close to the $\nu_3$ mode, ~200 $cm^{-1}$. However, this frequency is not compatible with calculated frequencies for the last totally symmetric mode, $\nu_2$. The doublet structure may thus originate from $\Delta v = 2$ excitation of a non-totally symmetric mode. As mentioned in Sec. IV B, the $\nu_4$ mode of the $Co_3O$ $^8A_1$ state is a good candidate for this behavior. In contrast, the $^{10}B_2$ state is a poor candidate; the non-totally symmetric modes are consistently above 137 $cm^{-1}$, consistent with harmonic behavior, and two-quanta excitation of any of these would be significantly larger than ~200 $cm^{-1}$.

The FC activity of the $\nu_4$ mode of the $Co_3O$ $^8A_1$ state is assessed by treating it as an anharmonic oscillator. A

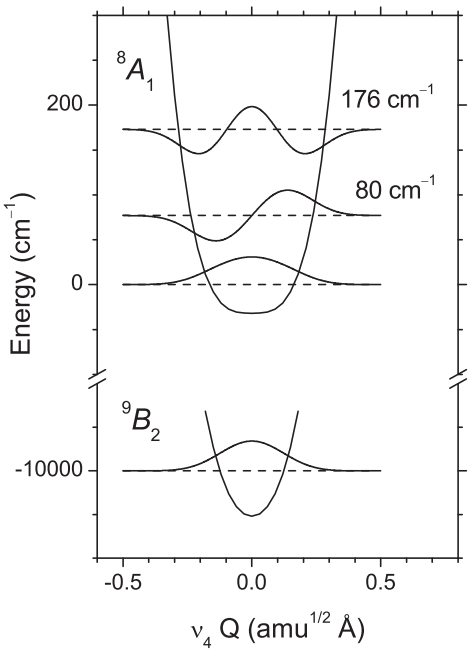


FIG. 8. 1D potential along the $b_1$ $\nu_4$ mode for the $Co_3O^-$ $^9B_2$ and $Co_3O$ $^8A_1$ species, calculated at TPSS/6-311+G*, with low-lying eigenenergies and energies.

one-dimensional slice along the normal coordinate for the $^8A_1$ and $^9B_2$ states was calculated at the TPSS/6-311+G* level, and eigenenergies and wavefunctions were solved numerically. As seen in Fig. 8, the flat potential near the $\nu_4$ minimum results in a negative anharmonicity in the neutral $^8A_1$ $Co_3O$. The fundamental $\nu_4$ is calculated to be 77 cm$^{-1}$ and $2\nu_4$ as 176 cm$^{-1}$, reasonably close to the ~200 cm$^{-1}$ of the unassigned vibrational excitation, and well within typical error of DFT vibrational frequencies for transition metal compounds.[67] The $4_0^2$ FC intensity $|\langle v' | v'' \rangle|^2$ was determined by direct integration. The $4_0^2$ $^8A_1 \leftarrow {}^9B_2$ transition is calculated to be 0.017 relative to the origin, a minor but appreciable amount. Peaks b–d can then be assigned as a $3_0^n 4_0^2$ (n = 0–2) progression, and peak f as the $1_0^1 4_0^2$ transition.

Overall, the SEVI spectra are most consistent with the $^8A_1 \leftarrow {}^9B_2$ transition. As with $Fe_3O^{0/-}$, these are the two lowest calculated states for the neutral and anion species, respectively. The calculated EA is ~1.26 eV (Table S1 in the supplementary material),[62] again in reasonable agreement with peak A at 1.3951 eV. We assign the main photodetachment band as the transition from the anion $\tilde{X}$ $^9B_2$ to the neutral $\tilde{X}$ $^8A_1$ ground states. The assigned states, electron affinity, and vibrational frequencies are summarized in Table III. Due to the expected anharmonicity of the $\nu_4$ mode, we report the $2\nu_4$ energy.

### C. Electronic states

The $M_3O$ clusters bind the excess anion electron in a largely metal 4*s* orbital. Detachment from the alpha HOMO of $Fe_3O^-$ and $Co_3O^-$ anions forms the corresponding ground state neutral species. This orbital looks very similar for the two different species (Fig. 9). It is largely centered on the metal atoms and is dominated by two in-plane lobes of opposite phase; the simple structure with one dominant node suggests that the orbital corresponds largely to a Fe or Co 4*s* weakly antibonding orbital, with electron density mostly on the oxo-bridged metal atoms. The orbitals do not have density centered directly over the metal atoms, suggesting polarization by the 4*p* orbitals. Natural Population Analysis seems to corroborate this assignment (Table S3 in the supplementary material).[62] The Fe 3*d* occupation is almost identical between the ground state anion and neutral species. However, the metal 4*p* and, even more so, the 4*s* occupation decreases upon electron detachment. Natural Population Analysis is not a reliable method for determining the precise metal 4*p* contribution in first-row transition metals, but qualitative trends should hold.[68,69]

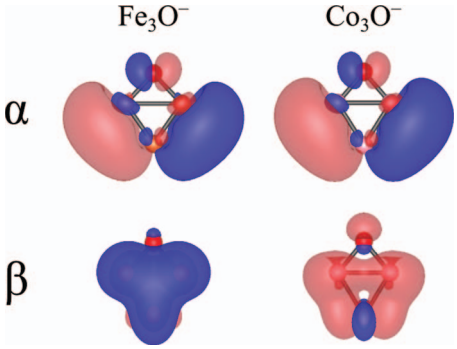


FIG. 9. Alpha and beta HOMOs of the $Fe_3O^-$ and $Co_3O^-$ anions.

Attachment of the excess electron in the metal valence *s* orbitals is consistent with other work. Upon electron attachment, all transition metal atoms with an unfilled valence *s* shell add the excess electron in that shell.[70] For the first row transition metal dimers, the most consistent assignments for the $Fe_2^-$, $Ni_2^-$, and $Cu_2^-$ photoelectron spectra have the excess electron largely in a 4*s* $\sigma_u$* orbital.[71–74] Previous calculations for larger $Fe_nO$ clusters found the anion alpha HOMO to have significant 4*s* character.[38] Analysis of the experimental photodetachment cross-sections of $V_3O^-$, $Nb_3O^-$, and $Ta_3O^-$ suggest that the excess electron is held in an orbital primarily of metal valence *s* character.[42] In general, metal and metal suboxide clusters seem to bind excess electrons in the *s* shell.

The electronic character of the detachment transitions is also consistent with both the geometry changes and the FC activity. Both the $Fe_3O^-$ and $Co_3O^-$ alpha HOMOs have some antibonding character between the oxo-bridged metals. As a result, the most significant calculated geometry change upon detachment is that the R2 bond length decreases by 0.05–0.07 Å. Similarly, the most FC-active mode should have significant symmetric stretching motion between the two oxo-bridged metal atoms; as shown in Fig. 5, this would be the $\nu_3$ mode, which is in fact the most active mode in both transitions. The excited $^{13}A_1$ state of $Fe_3O$ is accessed by detachment from the beta HOMO, a weakly bonding orbital with electron density on all three metal centers (Fig. 9 and Table S3 in the supplementary material).[62] Consequently, the major geometry change upon detachment is a metal trimer ring expansion; R2 and R3 are calculated to increase ~0.07 Å, and

the most active mode is the $\nu_2$ ring-breathing mode (Fig. 6), consistent with our assignments.

The overall spin states assigned are consistent with a picture of ferromagnetically coupled small iron and cobalt clusters. Stern-Gerlach magnetic deflection studies of size-selected iron and cobalt clusters have determined that almost all of these clusters are ferromagnetic, including neutral iron-oxo clusters.[41,75–81] Although there is considerable disagreement on the details, the overall consensus is that there is a typical spin magnetic contribution of ∼3 electrons per iron atom and ∼2 electrons per cobalt atom. The qualitative model used to explain this trend is based on band theory.[78] Low-coordinate regions like surfaces and defects form a large portion of small clusters, resulting in narrower bands than that for the bulk material. Upon promotion of a 4*s* electron to the 3*d* orbital, the larger 4*s* orbitals delocalize, forming a broad *s*-band and the majority of the metal bonding. The smaller 3*d* orbitals interact weakly and do not delocalize as much as the bulk 3*d* band or the low-coordinate 4*s* band. As a result, the observed magnetic moment is due to the spin excess in the 3*d* band as given by Hund's rules for the atoms.

Models based on band theory would not be expected to hold exactly for $Fe_3O$ and $Co_3O$; a trimer is a small cluster and the oxygen will perturb the electronic structure. Nonetheless, if the species can be considered ferromagnetic, these values should roughly hold true. Starting with atomic configurations of $[Ar](4s)^1(3d)^7$ and $[Ar](4s)^1(3d)^8$ for the three iron and cobalt atoms with $4s \rightarrow 3d$ promotion, the 3*d* band would have a spin excess of 9 and 6 electrons, respectively. The 4*s* band would have a doubly occupied bonding orbital and a singly occupied antibonding orbital, resulting in a final $2S + 1$ value of 11 and 8 for $Fe_3O$ and $Co_3O$. Remarkably, the neutral $Fe_3O$ and $Co_3O$ states are assigned exactly those spin multiplicities. The Natural Population Analysis also gives 3*d* occupations close to 7 and 8 for each iron and cobalt atom. The success of this simple model suggests that the single oxygen does not perturb the ferromagnetic behavior significantly. Previous low-resolution PE studies of various $Fe_nO^-$ and $Co_nO^-$ clusters also noted that the electron affinities were very similar to the corresponding pure metal clusters.[38,40,82]

### D. Comparison with prior work

The only prior experimental studies on the $M_3O^{0/-}$ (M = Fe, Co) clusters used conventional anion PE spectroscopy.[38–40] Due to lower resolution, around 30 meV, and likely higher ion temperatures, vibrational structure was not resolved. However, as the vibrational origin is strong, the onset of the ground state photodetachment band was clear in those experiments, yielding EAs of 1.44(2) eV for $Fe_3O$ and 1.38(8) eV for $Co_3O$. The earliest report on cobalt oxo clusters did not list a value for the EA of $Co_3O$, but the onset in the spectrum appears to be ∼1.3 eV.[40] These values are consistent with our more precise values of 1.4408(3) eV and 1.3951(4) eV, respectively. The vibrational assignments made in this work are the first reported experimentally for $Fe_3O$ and $Co_3O$.

Similar vibrational structure has been seen in vibrationally resolved photoelectron spectra of related metal oxide clusters, as mentioned in Section V A. High-resolution (sub-meV) photoionization spectra of neutral $Zr_3O$ and $Nb_3O$ were acquired by ZEKE,[37,43] and photoelectron spectra of $M_3O^-$ anions (M = V, Nb, Ta) were measured at 5–7 meV resolution.[42] Though the energy resolution in the anion PE study was not high as in the ZEKE and SEVI spectra, it was sufficient for assigning the observed vibrational structure.

All these studies observed a prominent origin and a short progression in the $\nu_3$ mode, with minor to negligible FC activity in the other totally symmetric modes. This overall FC profile is similar to that observed here for the $Fe_3O^-$ and $Co_3O^-$ SEVI spectra. The $\nu_3$ frequencies ranged from 215 to 355 $cm^{-1}$. The photodetachment spectra also showed minor FC activity in the $\nu_1$ mode, with frequencies 710–770 $cm^{-1}$. These frequencies are similar to but larger than our $\nu_1$ and $\nu_3$ frequencies for $Fe_3O$ and $Co_3O$ (Table III). This systematic difference is probably due to the weaker bonding in the clusters comprising the later transition-metal elements iron and cobalt compared to the earlier Group 4 and 5 metals. With a *d*-shell more than half full, there is more occupation in the metal antibonding orbitals, and the bond strength and force constants are diminished, as has been observed in the pure transition metal trimers.[83]

The experimental results are consistent with previous studies, but the electronic structure calculations are not. Although the same electronic structure program suite (Gaussian) and theory (BPW91/6-311+G*) were used, we have obtained different results than Gutsev *et al.*[38] and Li *et al.*[39] for the $Fe_3O^{0/-}$ and $Co_3O^{0/-}$ species. We obtain the same spin states corresponding to the ground state anion and neutral $Fe_3O$ with Gutsev *et al.* However, the relative energies of some states also differ by up to 0.2 eV. The geometries for the $Fe_3O^-$ dectet and dodectet states are also noticeably different; we find a planar dectet state while Gutsev *et al.* found a nonplanar state, and our calculated R2 bond lengths are shorter by 0.26 and 0.29 Å, respectively. These differences are significant, since our FC simulations show that the experimental $\nu_3$ vibrational structure is consistent with a ∼0.06 Å change in R2 upon photodetachment (Sec. V C), while Gutsev *et al.* predict a change of 0.25 Å, which would result in much more FC activity than that observed.

Our calculations for $Co_3O^{0/-}$ are also in qualitative agreement with those of Li *et al.*,[39] but there are again notable differences. As with $Fe_3O$, both reports found the same spin state and overall structure for the anion and neutral $Co_3O$. However, Co-Co bond lengths differ by ∼0.04 Å for both the anion and neutral species, the previous study obtained $C_s$-symmetric solutions while our ground states have $C_{2v}$ symmetry for both anion and neutral, and we could not reproduce the relative energies of the low-lying isomers. Li *et al.* located alternate structural isomers within 0.2 eV of the ground states for both the anion and neutral species, but we found those higher in energy by 0.54 and 0.33 eV, respectively. FC spectra for our lowest-energy alternate isomers of $Co_3O^{0/-}$ are shown in Fig. S1 in the supplementary material.[62] Both are poorer matches to the experiment than the assigned isomer and transition.

It is possible that the previous computational studies did not find the global SCF minima for all states. Depending on the initial guess, the SCF procedure may converge to a stationary point that is not the global minimum. While it is impossible to be absolutely sure whether a given solution corresponds to the global minimum, we used the wavefunction stability analysis program in Gaussian such that the final SCF solution at the optimized geometry is stable under the default perturbations considered. Moreover, we obtained similar results with two different functionals (Tables S1 and S2 in the supplementary material[62] and Fig. 4); though this does not guarantee a correct result, the internal self-consistency supports our confidence in our calculations. The differences from the previous calculations highlight the challenging nature of electronic structure calculations for transition metal systems.

## VI. CONCLUSIONS

We report high-resolution anion photoelectron spectra of $Fe_3O^-$ and $Co_3O^-$. The combination of ion trapping and cooling with the SEVI electron spectrometer allows for the acquisition of vibrationally well-resolved spectra of these systems for the first time, providing improved electron affinities and several new experimental vibrational frequencies for the neutral species. The electronic states of the anion and neutral species have been determined by comparison of calculated energies, FC simulations, and expected photoelectron anisotropies with the experimental spectra. Consistent with previous reports, on the basis of calculated energies and Franck-Condon intensities, the structural isomer of all ground state species is assigned to a triangular metal moiety with a $\mu_2$-oxo ligand.

Cold anion PE spectroscopy using SEVI can yield vibrationally well-resolved spectra of polymetal species. Assigning the important features, however, requires comparison with results from electronic structure calculations. In turn, it is difficult to obtain reliable results from calculations of polymetal species, but confidence in the results can be bolstered if spectroscopic and theoretical results are mutually self-consistent. SEVI can provide a rich set of experimental results, with photoelectron anisotropies, vibrational frequencies, detachment energies, and Franck-Condon profiles, all of which can be compared to theoretical expectations for different states, allowing us to assign electronic states and vibrational frequencies of anion and neutral metal oxide clusters.

## ACKNOWLEDGMENTS

This work is funded by the Air Force Office of Scientific Research under Grant No. FA9550-12-1-0160 and the Defense University Research Instrumentation Program under Grant No. FA9550-11-1-0330. M.L.W. thanks the National Science Foundation for a graduate research fellowship. We thank Nicholas J. Mayhall for a useful discussion of electronic structure methods for transition metal species.

[1]W. Weiss and W. Ranke, Prog. Surf. Sci. **70**, 1 (2002).
[2]Y.-F. Y. Yao, J. Catal. **33**, 108 (1974).
[3]X. Xie, Y. Li, Z.-Q. Liu, M. Haruta, and W. Shen, Nature (London) **458**, 746 (2009).
[4]D. G. Nocera, Acc. Chem. Res. **45**, 767 (2012).
[5]D. B. Jacobson and B. S. Freiser, J. Am. Chem. Soc. **108**, 27 (1986).
[6]S. K. Loh, L. Lian, and P. B. Armentrout, J. Chem. Phys. **91**, 6148 (1989).
[7]B. C. Guo, K. P. Kerns, and A. W. Castleman, J. Phys. Chem. **96**, 6931 (1992).
[8]M. Andersson, J. L. Persson, and A. Rosén, J. Phys. Chem. **100**, 12222 (1996).
[9]J. B. Griffin and P. B. Armentrout, J. Chem. Phys. **106**, 4448 (1997).
[10]E. Kapiloff and K. M. Ervin, J. Phys. Chem. A **101**, 8460 (1997).
[11]F. Liu, F.-X. Li, and P. B. Armentrout, J. Chem. Phys. **123**, 064304 (2005).
[12]G. E. Johnson, J. U. Reveles, N. M. Reilly, E. C. Tyo, S. N. Khanna, and A. W. Castleman, J. Phys. Chem. A **112**, 11330 (2008).
[13]J. U. Reveles, G. E. Johnson, S. N. Khanna, and A. W. Castleman, J. Phys. Chem. C **114**, 5438 (2010).
[14]N. M. Reilly, J. U. Reveles, G. E. Johnson, J. M. del Campo, S. N. Khanna, A. M. Köster, and A. W. Castleman, J. Phys. Chem. C **111**, 19086 (2007).
[15]N. M. Reilly, J. U. Reveles, G. E. Johnson, S. N. Khanna, and A. W. Castleman, J. Phys. Chem. A **111**, 4158 (2007).
[16]M. C. Oliveira, J. Marçalo, M. C. Vieira, and M. A. A. Ferreiraac, Int. J. Mass Spectrom. **185–187**, 825 (1999).
[17]W. Xue, Z.-C. Wang, S.-G. He, Y. Xie, and E. R. Bernstein, J. Am. Chem. Soc. **130**, 15879 (2008).
[18]Y. Xie, F. Dong, S. Heinbuch, J. J. Rocca, and E. R. Bernstein, J. Chem. Phys. **130**, 114306 (2009).
[19]Y. Xie, F. Dong, S. Heinbuch, J. J. Rocca, and E. R. Bernstein, Phys. Chem. Chem. Phys. **12**, 947 (2010).
[20]K. R. Asmis and J. Sauer, Mass Spectrom. Rev. **26**, 542 (2007).
[21]A. Fielicke, G. von Helden, G. Meijer, D. B. Pedersen, B. Simard, and D. M. Rayner, J. Am. Chem. Soc. **127**, 8416 (2005).
[22]R. O. Ramabhadran, J. E. Mann, S. E. Waller, D. W. Rothgeb, C. C. Jarrold, and K. Raghavachari, J. Am. Chem. Soc. **135**, 17039 (2013).
[23]A. J. Merer, Annu. Rev. Phys. Chem. **40**, 407 (1989).
[24]Y. Gong, M. Zhou, and L. Andrews, Chem. Rev. **109**, 6765 (2009).
[25]K. R. Asmis, Phys. Chem. Chem. Phys. **14**, 9270 (2012).
[26]K. M. Ervin and W. C. Lineberger, in *Advances in Gas Phase Ion Chemistry*, edited by N. G. Adams and L. M. Babcock (JAP Press, 1992), Vol. 1, p. 121.
[27]L.-S. Wang, in *Photoionization and Photodetachment*, edited by C. Y. Ng (World Scientific, Singapore, 2000), Vol. 10, p. 854.
[28]H.-J. Zhai and L.-S. Wang, Chem. Phys. Lett. **500**, 185 (2010).
[29]J. E. Mann, N. J. Mayhall, and C. C. Jarrold, Chem. Phys. Lett. **525–526**, 1 (2012).
[30]A. Osterwalder, M. J. Nee, J. Zhou, and D. M. Neumark, J. Chem. Phys. **121**, 6317 (2004).
[31]D. M. Neumark, J. Phys. Chem. A **112**, 13287 (2008).
[32]I. León, Z. Yang, H.-T. Liu, and L.-S. Wang, Rev. Sci. Instrum. **85**, 083106 (2014).
[33]J. B. Kim, M. L. Weichman, and D. M. Neumark, J. Chem. Phys. **140**, 034307 (2014).
[34]J. B. Kim, M. L. Weichman, and D. M. Neumark, J. Am. Chem. Soc. **136**, 7159 (2014).
[35]L. Wu, C. Zhang, S. A. Krasnokutski, and D.-S. Yang, J. Chem. Phys. **137**, 084312 (2012).
[36]L. Wu, C. Zhang, S. A. Krasnokutski, and D.-S. Yang, J. Chem. Phys. **140**, 224307 (2014).
[37]D.-S. Yang, Coord. Chem. Rev. **214**, 187 (2001).
[38]G. L. Gutsev, C. W. Bauschlicher, H.-J. Zhai, and L.-S. Wang, J. Chem. Phys. **119**, 11135 (2003).
[39]R.-Z. Li, J. Liang, X.-L. Xu, H.-G. Xu, and W.-J. Zheng, Chem. Phys. Lett. **575**, 12 (2013).
[40]H. Yoshida, A. Terasaki, and T. Kondow, Surf. Rev. Lett. **3**, 667 (1996).
[41]D. M. Cox, D. J. Trevor, R. L. Whetten, E. A. Rohlfing, and A. Kaldor, Phys. Rev. B **32**, 7290 (1985).
[42]S. M. E. Green, S. Alex, N. L. Fleischer, E. L. Millam, T. P. Marcy, and D. G. Leopold, J. Chem. Phys. **114**, 2653 (2001).
[43]D.-S. Yang, M. Z. Zgierski, D. M. Rayner, P. A. Hackett, A. Martinez, D. R. Salahub, P.-N. Roy, and T. Carrington, Jr., J. Chem. Phys. **103**, 5335 (1995).
[44]H. Shiroishi, T. Oda, I. Hamada, and N. Fujima, Eur. Phys. J. D **24**, 85 (2003).
[45]H. Shiroishi, T. Oda, I. Hamada, and N. Fujima, Polyhedron **24**, 2472 (2005).

[46]L. Liu, R.-N. Zhao, J.-G. Han, F.-Y. Liu, G.-Q. Pan, and L.-S. Sheng, J. Phys. Chem. A **113**, 360 (2009).
[47]R. H. Aguilera-del-Toro, F. Aguilera-Granja, A. Vega, and L. C. Balbás, Phys. Chem. Chem. Phys. **16**, 21732 (2014).
[48]C. Hock, J. B. Kim, M. L. Weichman, T. I. Yacovitch, and D. M. Neumark, J. Chem. Phys. **137**, 244201 (2012).
[49]A. T. J. B. Eppink and D. H. Parker, Rev. Sci. Instrum. **68**, 3477 (1997).
[50]B. Dick, Phys. Chem. Chem. Phys. **16**, 570 (2014).
[51]J. B. Kim, M. L. Weichman, T. I. Yacovitch, C. Shih, and D. M. Neumark, J. Chem. Phys. **139**, 104301 (2013).
[52]J. Cooper and R. N. Zare, J. Chem. Phys. **48**, 942 (1968).
[53]R. Mabbs, E. R. Grumbling, K. Pichugin, and A. Sanov, Chem. Soc. Rev. **38**, 2169 (2009).
[54]C. Bartels, C. Hock, J. Huwer, R. Kuhnen, J. Schwöbel, and B. von Issendorff, Science **323**, 1323 (2009).
[55]S. Dressler and W. Thiel, Chem. Phys. Lett. **273**, 71 (1997).
[56]S. E. Wheeler and K. N. Houk, J. Chem. Theory Comput. **6**, 395 (2010).
[57]M. J. Frisch, G. W. Trucks, H. B. Schlegel *et al.*, Gaussian 09, Revision C.01, Gaussian, Inc., Pittsburgh, PA, 2009.
[58]J. Tao, J. P. Perdew, V. N. Staroverov, and G. E. Scuseria, Phys. Rev. Lett. **91**, 146401 (2003).
[59]C. J. Cramer and D. G. Truhlar, Phys. Chem. Chem. Phys. **11**, 10757 (2009).
[60]T. M. Maier, A. D. Boese, J. Sauer, T. Wende, M. Fagiani, and K. R. Asmis, J. Chem. Phys. **140**, 204315 (2014).
[61]A. E. Reed, R. B. Weinstock, and F. Weinhold, J. Chem. Phys. **83**, 735 (1985).
[62]See supplementary material at http://dx.doi.org/10.1063/1.4900646 for details of calculated states, geometries, vibrational frequencies, the Natural Population Analysis, and FC simulations of alternate isomers.
[63]V. A. Mozhayskiy and A. I. Krylov, ezSpectrum, 2009, see http://iopenshell.usc.edu/downloads.
[64]E. P. Wigner, Phys. Rev. **73**, 1002 (1948).
[65]E. Surber, R. Mabbs, and A. Sanov, J. Phys. Chem. A **107**, 8215 (2003).
[66]K. J. Reed, A. H. Zimmerman, H. C. Anderson, and J. I. Brauman, J. Chem. Phys. **64**, 1368 (1976).
[67]C. J. Barden, J. C. Rienstra-Kiracofe, and H. F. Schaefer, J. Chem. Phys. **113**, 690 (2000).
[68]F. Maseras and K. Morokuma, Chem. Phys. Lett. **195**, 500 (1992).
[69]G. Frenking and N. Fröhlich, Chem. Rev. **100**, 717 (2000).
[70]T. Andersen, H. K. Haugen, and H. Hotop, J. Phys. Chem. Ref. Data **28**, 1511 (1999).
[71]D. G. Leopold, J. Almlöf, W. C. Lineberger, and P. R. Taylor, J. Chem. Phys. **88**, 3780 (1988).
[72]O. Hübner and J. Sauer, Chem. Phys. Lett. **358**, 442 (2002).
[73]J. Ho, K. M. Ervin, and W. C. Lineberger, J. Chem. Phys. **93**, 6987 (1990).
[74]J. Ho, M. L. Polak, K. M. Ervin, and W. C. Lineberger, J. Chem. Phys. **99**, 8542 (1993).
[75]J. P. Bucher, D. C. Douglass, and L. A. Bloomfield, Phys. Rev. Lett. **66**, 3052 (1991).
[76]D. C. Douglass, A. J. Cox, J. P. Bucher, and L. A. Bloomfield, Phys. Rev. B **47**, 12874 (1993).
[77]I. M. L. Billas, A. Châtelain, and W. A. de Heer, Science **265**, 1682 (1994).
[78]I. M. L. Billas, A. Châtelain, and W. A. de Heer, J. Magn. Magn. Mater. **168**, 64 (1997).
[79]M. B. Knickelbein, Chem. Phys. Lett. **353**, 221 (2002).
[80]M. B. Knickelbein, J. Chem. Phys. **125**, 044308 (2006).
[81]X. Xu, S. Yin, R. Moro, A. Liang, J. Bowlan, and W. A. de Heer, Phys. Rev. Lett. **107**, 057203 (2011).
[82]A. Pramann, K. Koyasu, A. Nakajima, and K. Kaya, J. Phys. Chem. A **106**, 4891 (2002).
[83]J. R. Lombardi and B. Davis, Chem. Rev. **102**, 2431 (2002).